Supporting Information for

Photochemical tyrosine oxidation in the structurally well-defined α_3Y protein: Proton-coupled electron transfer and a long-lived tyrosine radical

Starla D. Glover[1], Christine Jorge[2], Li Liang[2], Kathleen G. Valentine[2],

Leif Hammarström[1]* and Cecilia Tommos[2]*

1. Department of Chemistry – Ångström Laboratory, Uppsala University, Box 523, SE-75120 Uppsala, Sweden. 2. Graduate Group in Biochemistry & Molecular Biophysics and Department of Biochemistry & Biophysics, University of Pennsylvania, Philadelphia, Pennsylvania 19104-6059, U.S.A.

Index page

1. *Solvent accessible surface area (SASA) analysis of the α_3Y NMR structure*

The SASA analysis was performed on the 32-membered structural ensemble that represents the solution NMR structure of α_3Y using MOLMOL.[1] A solvent probe radius of 1.4 Å and a level 5 precision were used for the calculations. Core residues in heptad *a* and *d* positions are in color.

Table S1. Average solvent accessible surface areas of residues in α_3Y.

Residue	Heptad Position	Average SASA (%)	Residue	Heptad Position	Average SASA (%)
-2 GLY		47.6 ± 7.9	32 TYR	*a*	**0.2 ± 0.2**
-1 SER		44.6 ± 4.9	33 GLU	*b*	32.1 ± 3.7
1 ARG	*g*	32.5 ± 3.5	34 GLU	*c*	32.2 ± 4.6
2 VAL	*a*	3.8 ± 1.6	35 LEU	*d*	2.0 ± 1.1
3 LYS	*b*	39.5 ± 1.9	36 LYS	*e*	12.5 ± 3.7
4 ALA	*c*	23.8 ± 1.7	37 LYS	*f*	42.3 ± 4.1
5 LEU	*d*	3.0 ± 0.8	38 LYS	*g*	24.5 ± 4.0
6 GLU	*e*	10.7 ± 2.9	39 ILE	*a*	1.3 ± 0.3
7 GLU	*f*	37.6 ± 2.0	40 GLU	*b*	50.8 ± 2.1
8 LYS	*g*	28.1 ± 4.1	41 GLU	*c*	48.7 ± 4.8
9 VAL	*a*	0.1 ± 0.1	42 LEU	*d*	5.7 ± 2.0
10 LYS	*b*	30.6 ± 3.2	43 GLY		33.1 ± 5.9
11 ALA	*c*	29.2 ± 1.5	44 GLY		28.2 ± 8.6
12 LEU	*d*	10.9 ± 2.4	45 GLY		23.0 ± 6.5
13 GLU	*e*	12.7 ± 3.3	46 GLY		28.6 ± 6.2
14 GLU	*f*	36.1 ± 2.8	47 GLU	*g*	28.3 ± 4.3
15 LYS	*g*	26.6 ± 4.4	48 VAL	*a*	1.0 ± 0.9
16 VAL	*a*	0.0 ± 0.0	49 LYS	*b*	39.0 ± 2.9
17 LYS	*b*	38.2 ± 4.5	50 LYS	*c*	42.4 ± 4.1
18 ALA	*c*	36.8 ± 1.7	51 VAL	*d*	0.6 ± 0.6
19 LEU	*d*	18.0 ± 2.9	52 GLU	*e*	20.1 ± 2.6
20 GLY		21.4 ± 7.3	53 GLU	*f*	34.8 ± 5.2
21 GLY		29.5 ± 7.4	54 GLU	*g*	17.8 ± 4.3
22 GLY		30.0 ± 7.2	55 VAL	*a*	1.7 ± 1.2
23 GLY		23.9 ± 5.0	56 LYS	*b*	37.0 ± 3.7
24 ARG	*g*	38.6 ± 4.3	57 LYS	*c*	36.9 ± 5.2
25 ILE	*a*	5.2 ± 2.1	58 LEU	*d*	2.5 ± 1.8
26 GLU	*b*	25.6 ± 4.1	59 GLU	*e*	12.2 ± 3.5
27 GLU	*c*	34.6 ± 3.9	60 GLU	*f*	27.5 ± 3.6
28 LEU	*d*	5.1 ± 1.7	61 GLU	*g*	25.3 ± 3.8
29 LYS	*e*	17.4 ± 3.6	62 ILE	*a*	3.8 ± 1.7
30 LYS	*f*	41.7 ± 3.2	63 LYS	*b*	48.8 ± 4.3
31 LYS	*g*	36.7 ± 5.8	64 LYS	*c*	54.0 ± 3.2
			65 LEU	*d*	25.2 ± 2.8

2. *Chemical denaturation of α_3Y*

The global stability of α_3Y was determined by urea denaturation at pH 4.5, 8.5 and 9.9 (Figure S1). Experimental details are provided in the Materials and Methods section in the main manuscript. The data in Figure S1 complement earlier reports on the stability of α_3Y measured at pH 5.0, 5.5 and 8.2.[2,3] The global stability of α_3Y remains unchanged between pH 5.0 and 8.5 (–3.8 ± 0.1 kcal mol^{-1}) and is slightly lower at pH 4.5 (–3.3 ± 0.1 kcal mol^{-1}) and 9.9 (–3.5 ± 0.1 kcal mol^{-1}).

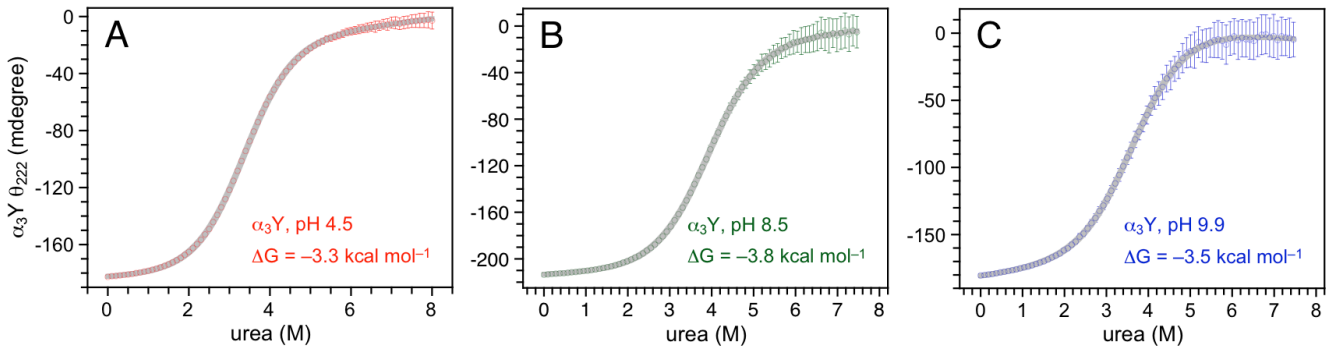

Figure S1. *Urea denaturation of α_3Y at (A) pH 4.5, (B) pH 8.5 and (C) pH 9.9. The grey lines represent nonlinear fits to determine the stability of the protein in the absence of urea.[4] The average standard error in the reported ΔG values is ± 0.1 kcal mol^{-1}.*

3. *Characterization of cobalt phosphate/oxide precipitates*

As shown in Figure 2 in the main manuscript, kinetic traces collected on long timescales (>1 s) display a baseline offset. Transient absorption (TA) properties of the $[Ru(bpy)_3]Cl_2$ sensitizer and the $[Co(NH_3)_5Cl]Cl_2$ quencher were assessed in the absence of the α_3Y protein. These control experiments show that the observed baseline is due to light absorbing/scattering products formed in reactions between Co^{2+} (from decomposed quencher) and buffer ions, phosphate as well as borate. Spectra of solutions containing $[Ru(bpy)_3]Cl_2$ and $[Co(NH_3)_5Cl]Cl_2$ at pH 5.5 (Figure S2A) and pH 8.5 (Figure S2B) were recorded at different time intervals on a diode array spectrometer. Kinetics traces of pH 5.5 and 8.5 solutions from laser flash photolysis experiments are shown in Figures 3a and 3c in the main text (grey traces). A FTIR spectrum of precipitates that were isolated after a flash photolysis experiment is shown in Figure S3. Infrared spectra were indistinguishable for precipitates collected from experiments performed with or without α_3Y at both pH 5.5 and 8.5.

The difference spectra at pH 5.5 (Figure S2A) were collected in an identical fashion to the Y32-O• spectra (Figure 2, main manuscript). The displayed spectra correspond to the light-minus-dark difference observed at 2.5 s, 5 s and 26 minutes after the flash of light. The initial $Ru(bpy)^{2+}$ bleach appears at ~450 nm and does not fully recover over the course of the study due to the irreversibility of the quencher. The positive signal that covers the visible spectrum after 26 minutes is due to precipitated material and appears as broad and featureless from scattering of the probe light. The sample at pH 8.5 (Figure S2B) was not subject to a pulse of excitation light, yet the formation of the

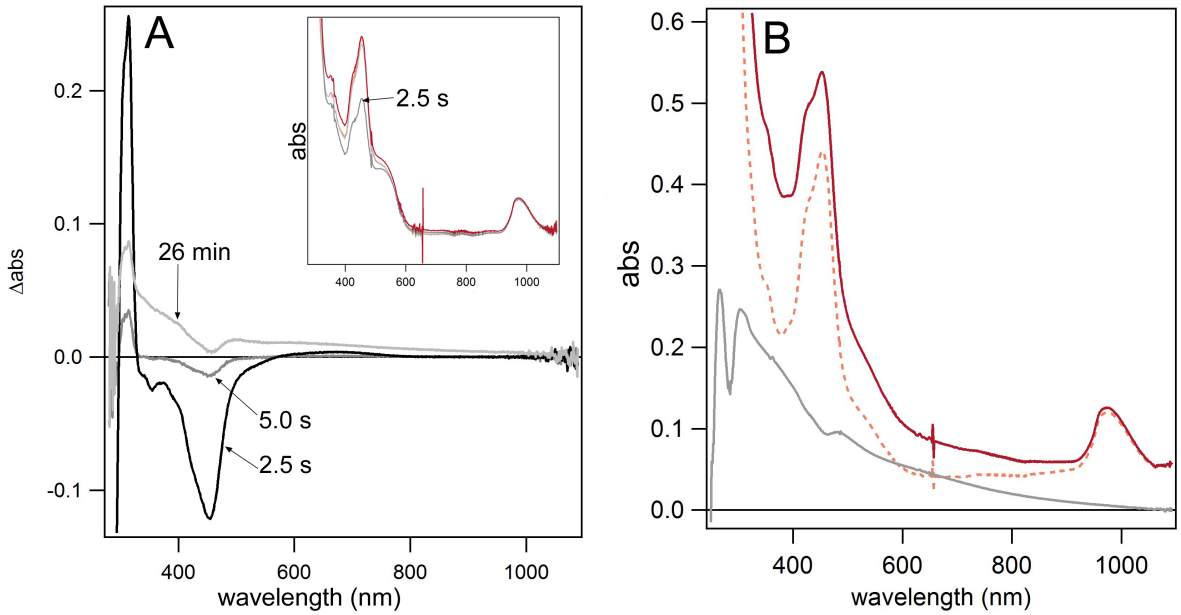

Figure S2. *Control experiments with no α_3Y after irradiation of a sample containing $[Ru(bpy)_3]Cl_2$ and $[Co(NH_3)_5Cl]Cl_2$. Shown are difference spectra of a $[Ru(bpy)_3]Cl_2$ and $[Co(NH_3)_5Cl]Cl_2$ sample at (A) pH 5.5 and (B) pH 8.5. The inset in panel (A) shows the raw spectra that were used to generate the difference spectra. Panel (B) shows the first spectrum collected at the start of the experiment (orange dotted line), the last spectrum (red line), and the corresponding difference spectrum (grey line). Sample conditions: 45 μM $[Ru(bpy)_3]Cl_2$ and 2 mM $[Co(NH_3)_5Cl]Cl_2$ in 20 mM PB buffer, 40 mM KCl.*

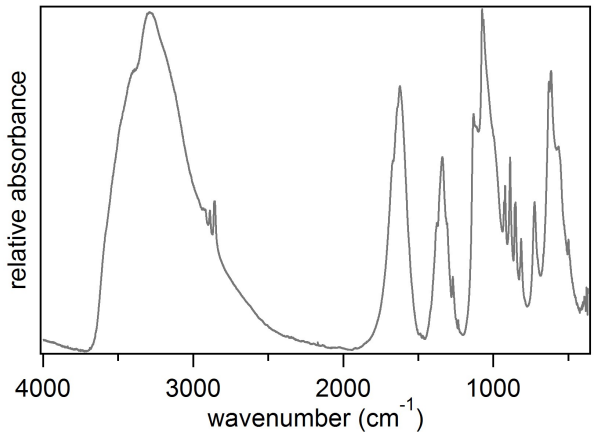

Figure S3. *Representative infrared spectrum of precipitated products formed during a flash photolysis experiment. The spectrum shows peaks associated with water and phosphate stretches: intense bands due to water at ~3300 and 1630 cm^{-1} and medium bands due to PO_4^{3-} at 1050, 630, 615 and 564 cm^{-1}. A medium band at 1340 cm^{-1} is consistent with borate and provides evidence that borate salt is also part of the precipitates. The small stretches at ~2900 cm^{-1} in the shoulder of the water band are consistent with small amounts of 2,2'-bipyridine from decomposed sensitizer. Sample Preparation: Spent flash photolysis solutions containing precipitates were centrifuged and the supernatant removed. The solids were washed and centrifuged 5 times with high purity water to remove soluble material and buffer salts. The solids were dried in vacuo for 12 h and then pressed into a KBr matrix.*

precipitates was observed. The probe light of the diode array excites the sensitizer and drives the precipitate forming reactions. The initial and final spectra are the orange dotted and red solid line, respectively, while the difference spectrum is shown in grey. Again, the difference spectrum shows the absorption/light scattering profile of the precipitated material.

Flash photolysis experiments in the absence of α_3Y (Figures 3a and 3c, main manuscript) show that transient absorption kinetic profile of these absorbing species is negligible on the ms timescale. Their formation is so slow that their impact on the α_3Y and L-tyrosine kinetics (k_{obs}) would present only a minimal contribution.

4. *Kinetic fits and simulations*

Tyrosine radicals can be detected from their absorption at 410 nm (see Figure 2, main manuscript). At this wavelength, the Ru^{2+} bleach is also apparent. Transient absorption traces collected at 410 nm thus report on Ru^{2+} recovery as well as the formation of Y-O• (i.e. they provide information on k_{PCET} associated with tyrosine oxidation and the Y-O• yield). Should Y-O• dimerize or be subject to other side reactions, the 410 nm signal will diminish in intensity. When the oxidation reaction is fast relative to the radical side reaction(s), the amplitude of the signal at 410 nm can reflect a Y-O• yield of 100%. Such is the case for the TA signal of L-tyrosine at pH 8.5, which displays a maximum positive amplitude at 410 nm that is ~2/3 of the Ru^{2+} bleach at the same wavelength. The 2/3 factor comes from the ratio of ε_{410}(Y-O•) and $\Delta\varepsilon_{410}(Ru^{2+})$, which are 3000 and 4500 $M^{-1}cm^{-1}$, respectively.[5,6] Figure 4B in the main manuscript shows the fitting result of the 410 nm TA signal for L-tyrosine at pH 8.5 applying a model of a pseudo-first order recovery ([Y-OH] >> [Ru^{3+}]) followed by a second order decay.

$$\text{Y-OH} + Ru^{3+} \rightarrow \text{Y-O•} + Ru^{2+} + H^+$$

$$2\text{Y-O•} \rightarrow Y_{dim}$$

The concentrations of Ru^{3+}, Y-O•, and Y_{dim} as a function of time can be described by the following system of equations:

$$\frac{d[Ru^{3+}]}{dt} = -k_1[Ru^{3+}] \quad (1)$$

$$\frac{d[YO•]}{dt} = k_1[Ru^{3+}] - 2k_2[YO\ •]^2 \quad (2)$$

$$\frac{d[Y_{dim}]}{dt} = k_2[YO\ •]^2 \quad (3)$$

The non-trivial analytical solution describing [Y-O•] as a function of time has been reported.[7,8] In this model [Y-O•] as a function of time depends on three parameters: the initial Ru^{3+} concentration, the pseudo-first order rate constant, k_1, and the second order rate constant, k_2. The k_1 and k_2 rate constants are reported as k_{obs} and $k_{Y\text{-}O\bullet}$ in Table 2 of the main manuscript, respectively. The TA signal at 410 nm is reproduced by the sum of the contributions of the recovering Ru^{2+} signal (solution to equation 1) and

the Y-O• signal (solution to equation 2). At 450 nm the $Ru(bpy)_3^{2+}$ bleach is stronger and the Y-O• absorption is weaker than at 410 nm. As pointed out in the main article, a single exponential fit to the 450 nm traces, reflecting (1) above, gave values of k_{obs} that were the same as those derived at 410 nm.

Figure 4A in the main manuscript shows the fitting result for L-tyrosine at pH 5.5 using the same model. In this case the rate of PCET that generates Y-O• is slower and the effect of the second order decay process is apparent. Thus the maximum positive amplitude of the 410 signal at pH 5.5 is significantly less than that of the maximum signal at pH 8.5. Despite the diminished 410 nm maximum amplitude at pH 5.5 the trace is consistent with 100% yield of Y-O• with respect to Ru^{3+} generated per laser flash. At pH 5.5 conditions the lower amplitude of the 410 nm signal is simply due to concurrent tyrosine oxidation and radical-radical dimerization. The experimentally determined rates k_{obs} and $k_{Y\text{-}O\bullet}$ from Table 2 in the main manuscript were treated as constant fitting parameters while the yield of Y32-O•, Yield(Y32-O•), was a floating parameter. The resulting fits for L-tyrosine at pH 5.5 and 8.5 are shown in Figure 4. k_{PCET} was determined from the following relationships: $k_{obs} = [\alpha_3Y]\times k_{PCET} + [X]\times k_{COMP}$ and $Yield(Y32\text{-}O\bullet) = [\alpha_3Y]\times k_{PCET}/k_{obs}$. In the case of L-tyrosine there was no competitive quencher, thus $k_{obs} = [Y]\times k_{PCET}$.

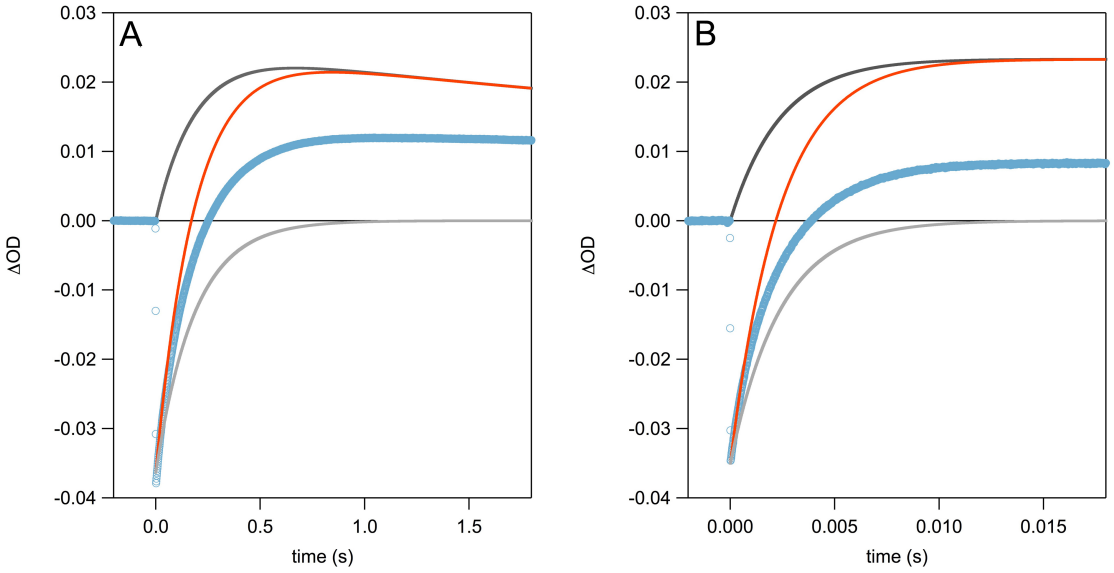

Figure S4. *Data simulations assuming a 100% yield of Y32-O• using a model of pseudo-first order growth followed by second order decay for the 410 nm TA traces collected from α_3Y at two different experimental conditions. Experimental TA traces are shown in blue and the corresponding simulations in orange. The light grey and dark grey lines represent the Ru^{2+} and Y-O• contributions to the 410 nm signal as a function of time, respectively. Simulated 410 nm TA traces for (A) 170 μM α_3Y at pH 5.5 and (B) 890 μM α_3Y at pH 8.5.*

The fitting routine described above was applied to the 410 nm TA signals that were recorded for α_3Y at pH(D) 5.5 and 8.5 in H_2O and in D_2O. Comparing the α_3Y kinetics at these four different sample conditions revealed that Y32-O• yield is not 100% under any of the conditions studied. Figure S4 displays simulated 410 nm TA traces (orange lines) that include the experimentally determined k_{obs} and $k_{Y\text{-}O\bullet}$ values in Table 2 (main manuscript) and a 100% Y32-O• yield at pH 5.5 and 8.5,

respectively. The radical yield is given relative to the flash-generated concentration of $[Ru(bpy)_3]^{3+}$. These simulations show that the Y32-O• yield is less than unity.

Figures S5A-F show TA traces at 410 nm and fits using the first order followed by second order kinetic model for α_3Y at all pH(D) and protein concentration conditions that are not shown in the main manuscript. Specifics regarding each trace are given in the figure caption. The yield of Y32-O• was found to be ca. 40%, 35%, 58% and 50% for pH 8.5, pD 8.5, pH 5.5 and pD 5.5, respectively.

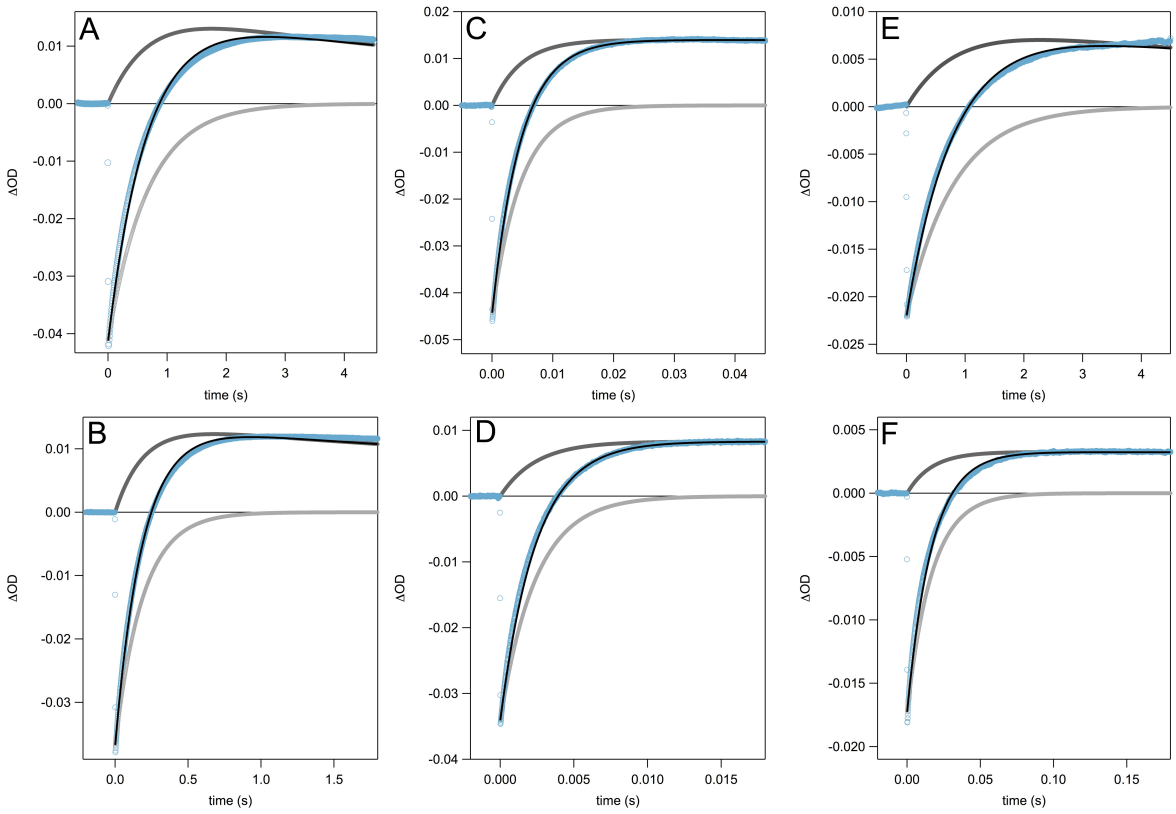

Figure S5. *Transient absorption traces along with fits for pseudo-first order recovery followed by second order decay. TA traces are given in blue while fits are given in black. Included are the contributions to the 410 signal from* Ru^{2+} *and Y32-O• in light grey and dark grey, respectively. The conditions are as follows: (A) 70 μM* α_3*Y in pH 5.5 buffer, (B) 170 μM* α_3*Y in pH 5.5 buffer, (C) 580 μM* α_3*Y in pH 8.5 buffer, (D) 890 μM* α_3*Y in pH 8.5 buffer, (E) 150 μM* α_3*Y in pD 5.5 buffer, and (F) 480 μM* α_3*Y in pD 8.5 buffer.*

5. *α_3F/trifluoroacetic acid control studies*

A ns flash photolysis control study was performed with α_3F in lieu of α_3Y to assess the reactivity of the protein scaffold. The F32 residue in α_3F is expected to be redox inert under the conditions employed in this study, and any photochemical reactivity from the protein scaffold should be apparent. The experimental conditions used in this control experiment were identical to the conditions used for the α_3Y flash photolysis experiments. Inspection of each plot in Figure S6 shows that after 4–5 laser shots the α_3F samples give the same response as samples containing only $[Ru(bpy)_3]Cl_2$ and $[Co(NH_3)_5Cl]Cl_2$ in buffered solution. Any reactivity from α_3F would give many reproducible traces on account of the relatively high concentration of protein (300 μM) versus the concentration of $[Ru(bpy)_3]^{3+}$ generated via a laser flash (3-9 μM). The data shown in Figure S6 verifies that the α_3 protein scaffold is unreactive under the present experimental conditions.

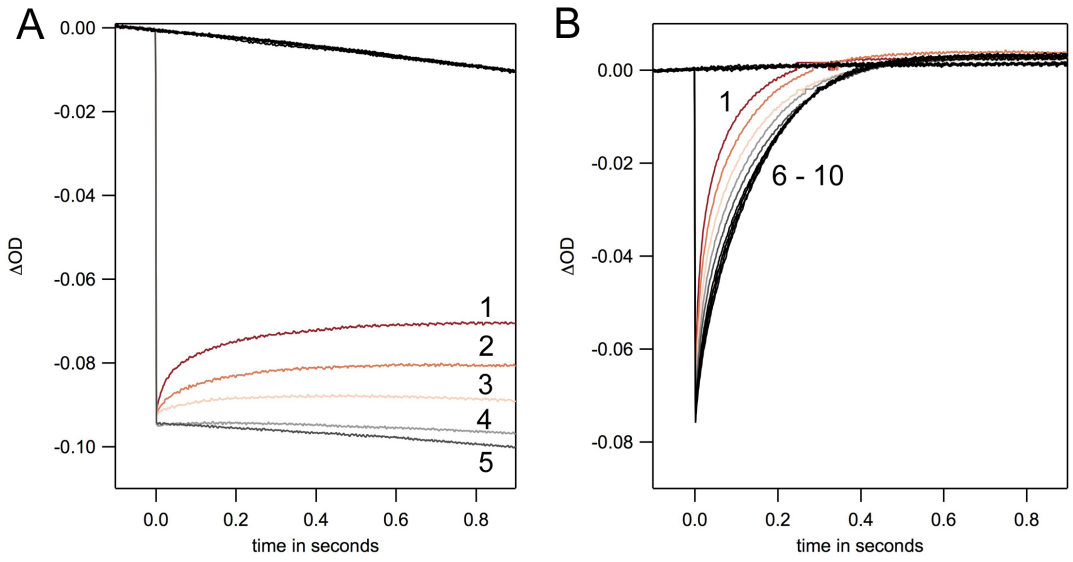

Figure S6. *(A) Laser flash photolysis experiment with α_3F at pH 5.5. The first five shots to the sample are correspondingly labeled. The traces shown in black are the systems response when there is no laser flash. (B) Laser flash photolysis experiment with α_3F at pH 8.5 where 10 shots were collected. After the sixth shot no significant changes can be detected.*

An additional control experiment was performed with 7 and 13 mM trifluoroacetic acid (TFA) at pH 5.5 and 8.5, respectively, where the flash photolysis solutions contained no protein. The kinetic response with subsequent shots (Figure S7) is strikingly similar to the solutions containing α_3F (Figure S6). As with α_3F, any reactivity from TFA itself would give reproducible shots on account of the high concentration of TFA *versus* $[Ru(bpy)_3]^{3+}$. Thus, a likely candidate for the competitive consumption of $[Ru(bpy)_3]^{3+}$ in flash photolysis experiments is a small impurity present in the TFA.

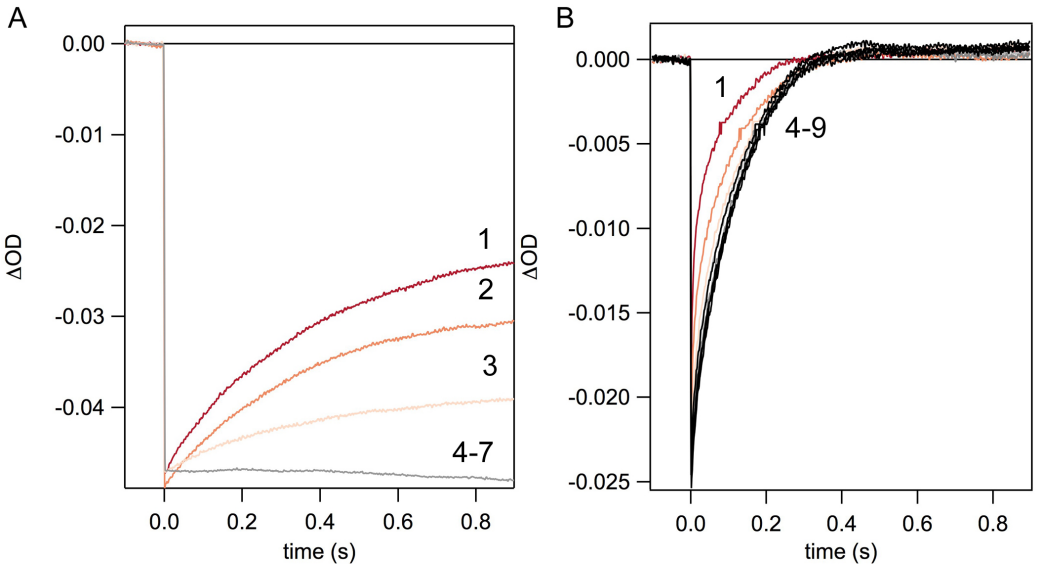

Figure S7. *Control study with trifluoroacetic acid (TFA) at (A) pH 5.5 and (B) pH 8.5. No α_3X protein is present in either sample. After 3 laser shots these samples give the same response as a solution containing only $[Ru(bpy)_3]Cl_2$ and $[Co(NH_3)_5Cl]Cl_2$ in buffered solution.*

6. *Transient absorption kinetic traces for Y32-O• decay*

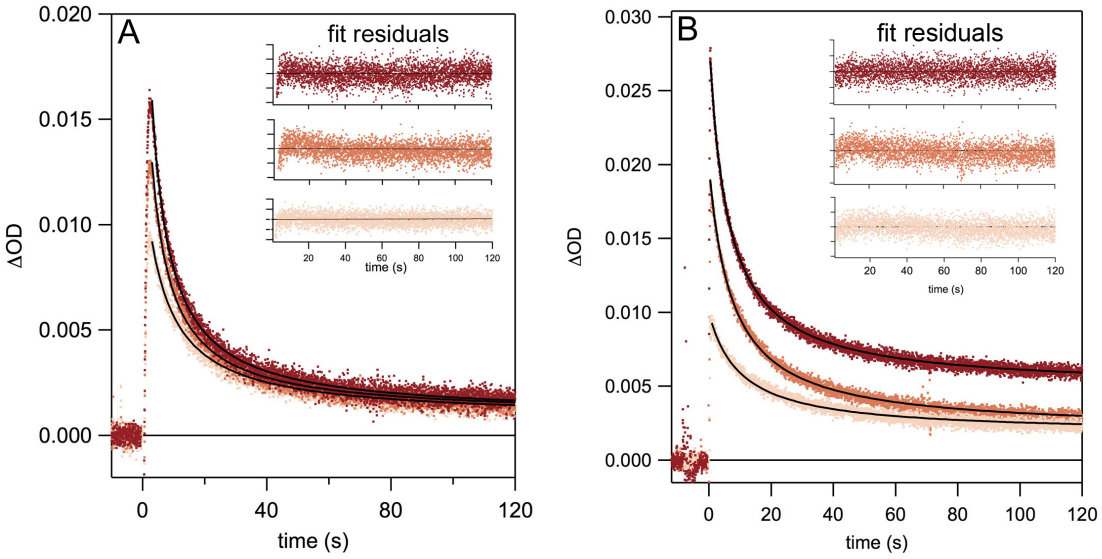

Figure S8. *Long timescale traces following the 410 nm absorption of Y32-O• at (A) pH 5.5 and (B) pH 8.5. Different initial concentrations of Y32-O• were generated by supplying the sample with an excitation pulse with a duration of 500 ms (red), 250 ms (orange), and 100 ms (beige). Global fitting to a second order rate constant yielded an average rate of decay of (1.4 ± 0.3) and (1.1 ± 0.3)×10^4 $M^{-1}s^{-1}$ for pH 5.5 and 8.5, respectively. The halftime for this reaction is taken to be $t_{1/2} = 1/k_2[Y32\text{-}O\bullet]_0$. The halftime was found to increase with decreasing $[Y32\text{-}O\bullet]_0$ values such that $t_{1/2}$(pH 5.5) was 5, 6, and 9 s for 13 (red), 10 (orange), and 8 (beige) μM initial Y32-O• concentrations and $t_{1/2}$(pH 8.5) was 4.4, 6.2, and 12 s for 18 (red), 13 (orange), and 6 (beige) μM initial Y32-O• concentrations, respectively.*

Table S2 contains the details for the transient absorption measurements where the initial concentration of Y32-O• was varied by the use of neutral density filters and a 500 ms excitation pulse. With the exception of the TA trace with the smallest initial concentration, the second order rate constants from this experiment are comparable to those from experiments where the initial concentration was varied by lengthening the pulse duration (Figure S8). The pH 5.5 solution had the following concentrations: 70 μM α_3Y, 30 μM $[Ru(bpy)_3]Cl_2$ and 2 mM $[Co(NH_3)_5Cl]Cl_2$.

Table S2. Decay kinetics of Y32-O• under varying initial concentrations.

$[Y32\text{-}O\bullet]_0$ (μM)	k_2 ($M^{-1}s^{-1}$)	$t_{1/2}$ (s)
34	$(1.4\pm0.2)\times10^4$	2
21	$(1.5\pm0.2)\times10^4$	3
16	$(1.7\pm0.2)\times10^4$	4
3	$(3.4\pm0.3)\times10^4$	10

7. *Steady state absorption and fluorescence control spectra*

Steady state fluorescence measurements were performed on a Horiba Jobin Yvon Fluorolog 3-222 fluorimeter configured with double-monochromators for excitation and emission with slits set to 1.0 nm resolution. Excitation wavelengths were 277, 305, 310 or 325 nm and emission was detected at a right angle with a R928P PMT detector in single photon counting mode such that the detected light gave a linear PMT response. The excitation fluorescence spectrum of α_3Y flash photolysis protein products was excited at 450 nm, in the red edge of the emission peak. All spectra were corrected for the wavelength sensitivity of the detector. Six different samples were investigated for fluorescent behavior: (i) unreacted α_3Y, (ii) α_3Y flash photolysis products, (iii) L-tyrosine flash photolysis products, (iv) $[Ru(bpy)_3]Cl_2$, (v) $[Co(NH_3)_5Cl]Cl_2$, and (vi) flash photolysis products of $[Ru(bpy)_3]Cl_2$ and $[Co(NH_3)_5Cl]Cl_2$. With the exception of the α_3Y flash photolysis products, all solutions were prepared with the same solvent as was used in transient absorption measurements and adjusted to pH 8.5. Prior to emission measurements, the α_3Y flash photolysis protein products were dialyzed (3500 molecular weight cut-off) in 20 mM potassium phosphate, pH 7.0. L-tyrosine photoproducts were filtered prior to emission measurements to remove cobalt phosphate/oxide particles. No further purification was necessary as the other contents of the solution, namely $[Ru(bpy)_3]Cl_2$, $[Co(NH_3)_5Cl]Cl_2$, $Ru(bpy)_3]Cl_2$ and $[Co(NH_3)_5Cl]Cl_2$ products, and buffer did not emit when excited under the conditions of this study (Figure S9, panel F).

Dityrosines exhibit a diagnostic emission spectrum with a maximum at ca. 400 nm when excited at 310-325 nm.[9-11] Fluorescence spectroscopy of both the isolated Y32-O• reaction products (Figure S9B) and L-tyrosine reaction products (Figure S9C) showed this characteristic emission while unreacted α_3Y, $[Ru(bpy)_3]Cl_2$, $[Co(NH_3)_5Cl]Cl_2$, $[Ru(bpy)_3]Cl_2$ and $[Co(NH_3)_5Cl]Cl_2$ products, and buffer did not emit under the same conditions. The emission spectra for Y32-O• reaction products and L-tyrosine reaction products match previously reported spectra for dityrosine. Further, the absorbance (Figure S9A) and fluorescence excitation spectrum (Figure S9D) of Y32-O• reaction products show the same

structural features that have been reported previously for dityrosine at pH ~7.[12] The series of absorption and fluorescence spectra displayed in Figure S9 verify that Y32-O• flash photolysis products exhibit the characteristic spectral properties of dityrosine.

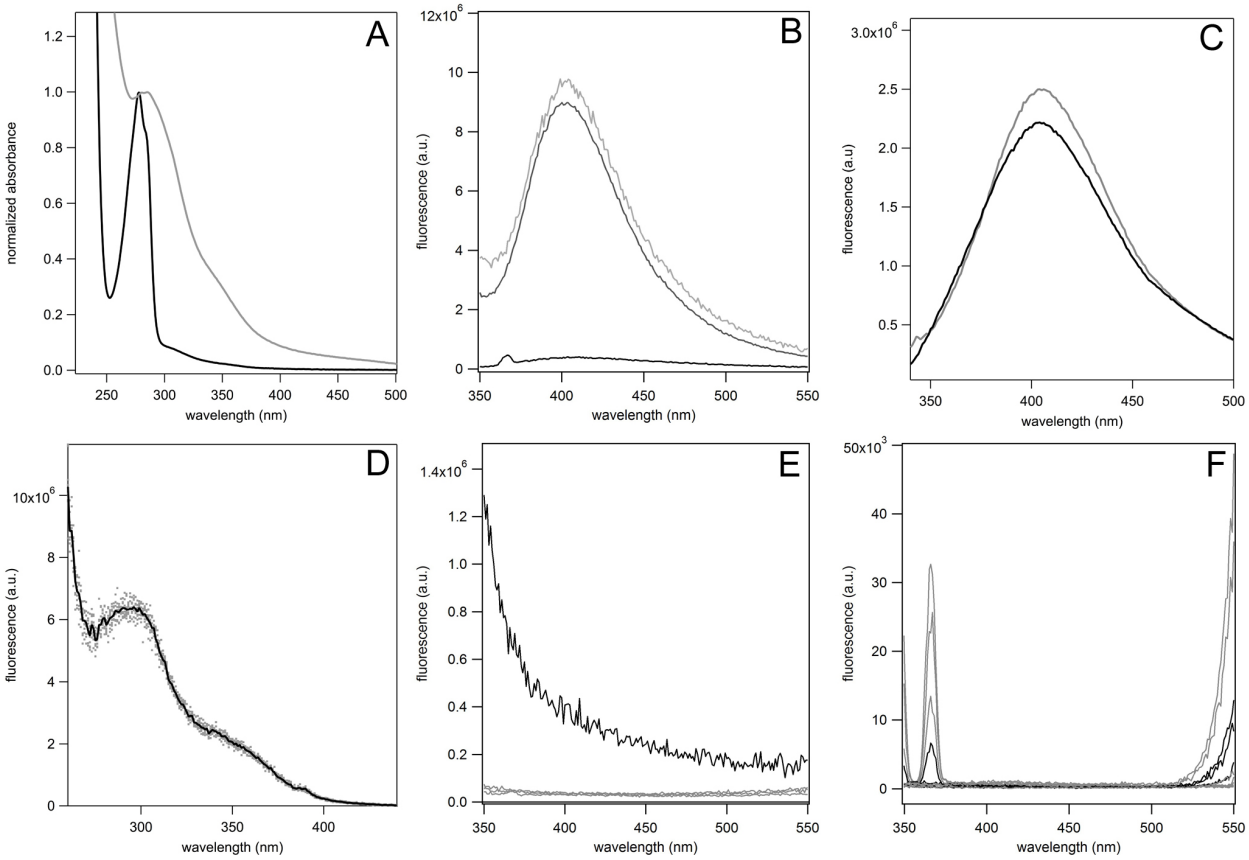

Figure S9. *(A) Normalized steady state absorption spectrum for unreacted α_3Y (black) and α_3Y flash photolysis products (grey). (B) Emission spectra of α_3Y flash photolysis products when excited at 325 nm (black), 310 nm (medium grey) and 277 nm (light grey). (C) Emission spectra for L-tyrosine flash photolysis products when excited at 305 nm (grey) and 325 nm (black). (D) Excitation spectrum for α_3Y flash photolysis products when excited at 450 nm. (E) Emission spectra for unreacted α_3Y at 325 nm and 310 nm (grey) and 277 nm (black). The intensity observed when α_3Y is excited at 277 nm is the tail region of the characteristic emission of tyrosine, which is centered at 301 nm for Y322.[2] Unreacted α_3Y does not emit when excited at 310 and 325 nm. (F) Emission spectra of four different solutions: $[Ru(bpy)_3]Cl_2$, $[Co(NH_3)_5Cl]Cl_2$, $[Ru(bpy)_3]Cl_2$ and $[Co(NH_3)_5Cl]Cl_2$ flash photolysis products, and buffer. The sharp peaks that appear at ~370 nm are solvent Raman lines and the rising absorption after 500 nm is due to emission by $*Ru(bpy)_3^{2+}$.*

8. α_3Y/[Ru(bpy)$_3$]Cl$_2$/[Co(NH$_3$)$_5$Cl]Cl$_2$ protein control studies

Circular dichroism (CD) spectroscopy and size-exclusion chromatography studies were conducted to investigate if the helical content and the monomeric[2] aggregation state of α_3Y change in the presence of the [Ru(bpy)$_3$]Cl$_2$ photosensitizer or the [Co(NH$_3$)$_5$Cl]Cl$_2$ oxidative quencher. α_3Y was dissolved in 20 mM potassium, 20 mM sodium borate, pH 7.0, and diluted to 60 μM in buffer only (Fig. S10A, red spectrum) and in buffer containing 40 μM [Ru(bpy)$_3$]Cl$_2$ (blue spectrum). The 222 nm ellipticity, which directly reflects the helicity of α_3Y, is the same in the two spectra. Due to total light absorption and/or scattering, CD spectra could not be collected on samples containing [Co(NH$_3$)$_5$Cl]Cl$_2$. Gel filtration samples were prepared from a 600 μM α_3Y solution diluted to 300 μM protein in buffer only (Fig. S10B), or buffer containing 40 μM [Ru(bpy)$_3$]Cl$_2$ (panel C), or 4 mM [Co(NH$_3$)$_5$Cl]Cl$_2$ (panel D). Monomeric[2] α_3Y elutes around 13.2 ml and there is no evidence of higher aggregation states, which would elute at smaller elution volumes. The 280 nm absorption of the free sensitizer and quencher is observed in panels C and D, as expected. We conclude that the protein properties of α_3Y are not perturbed by [Ru(bpy)$_3$]$^{2+}$ or [Co(NH$_3$)$_5$Cl]$^{2+}$ at the concentrations used in the flash-quench experiments.

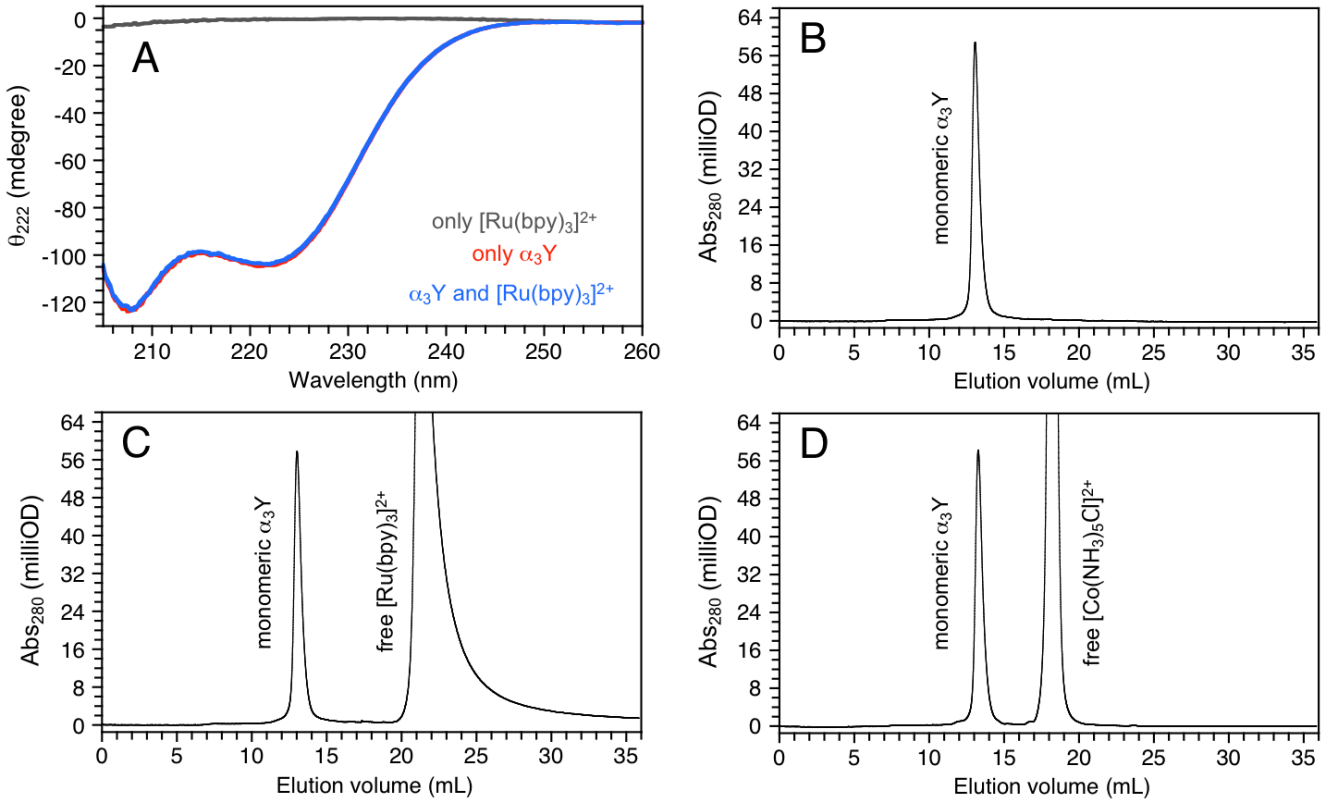

Figure S10. *(A) Circular dichroism spectra collected on samples containing 40 μM [Ru(bpy)$_3$]Cl$_2$ (dark grey), 60 μM α_3Y (red), and 60 μM α_3Y, 40 μM [Ru(bpy)$_3$]Cl$_2$ (blue). The CD spectra were recorded at 25 °C in a 1 mm path length cuvette. Analytical gel filtration chromatograms collected on samples containing B) 300 μM α_3Y, C) 300 μM α_3Y, 40 μM [Ru(bpy)$_3$]Cl$_2$, and D) 300 μM α_3Y, 4 mM [Co(NH$_3$)$_5$Cl]Cl$_2$. The column was equilibrated in sample buffer containing 20 mM potassium phosphate, 20 mM sodium borate, 40 mM KCl, pH 7.0.*

REFERENCES

(1) Koradi, R.; Billeter, M.; Wuthrich, K. *J. Mol. Graph.* **1996**, *14*, 51-52.

(2) Martinéz-Rivera, M. C.; Berry, B. W.; Valentine, K. G.; Westerlund, K.; Hay, S.; Tommos, C. *J. Am. Chem. Soc.* **2011**, *133*, 17786-17795.

(3) Ravichandran, K. R.; Liang, L.; Stubbe, J.; Tommos, C. *Biochemistry* **2013**, *52*, 8907-8915.

(4) Santoro, M. M.; Bolen, D. W. *Biochemistry* **1988**, *27*, 8063-8068.

(5) Magnuson, A.; Berglund, H.; Korall, P.; Hammarström, L.; Åkermark, B.; Styring, S.; Sun, L. C. *J. Am. Chem. Soc.* **1997**, *119*, 10720-10725.

(6) From the value $\varepsilon_{450}(Ru^{3+}) - \varepsilon_{450}(Ru^{2+}) = 10000\ M^{-1}cm^{-1}$ and the 2.2. times smaller initial bleach at 410 nm in reference 5 and the present study, we calculate $\varepsilon_{410}(Ru^{3+}) - \varepsilon_{410}(Ru^{2+}) = 4500\ M^{-1}\ cm^{-1}$.

(7) Chien, J. Y. *Kinetic Analysis of Irreversible Consecutive Reactions* **1948**, *70*, 2256-2261.

(8) Steinfeld, J. I.; Francisco, J. S.; Hase, W. L. *Chemical Kinetics and Dynamics*; 2nd ed.; Prentice-Hall: Upper Saddle River, New Jersey, **1998**.

(9) Gillard, N.; Goffinont, S.; Bure, C.; Davidkova, M.; Maurizot, J. C.; Cadene, M.; Spotheim-Maurizot, M. *Biochem. J.* **2007**, *403*, 463-472.

(10) Chakraborty, M.; Bhattacharya, D.; Mukhopadhyay, C.; Chakrabarti, A. *Biophys. Chem.* **2010**, *149*, 92-101.

(11) Marquez, L. A.; Dunford, H. B. *J. Biol. Chem.* **1995**, 270, 30434-30440.

(12) Kungl, A. J.; Landl, G.; Visser, J. W. G. A.; Breitenbach, M.; Kauffmann, H. F. J. *Fluorescence* **1992**, 1, 63-74.